



Fabrication and Characterization of Rice Straw-Derived Cellulose Nanofibers for Enhanced Adsorption of Reactive Black 5 and Methylene Blue Dyes from Aqueous Solutions

Ghada A. Amin¹, Ghada A. Kadry², Taha M. A. Razek¹, and Ahmed G. Hassabo^{3*}

¹ Department of Environmental Basic Science, Faculty of Environmental Studies and Research, Ain Shams University, Cairo, Egypt

² Chemical Engineering Department, Higher Institute of Engineering, El-Shorouk Academy, Cairo, Egypt

³ National Research Centre (NRC, Scopus affiliation ID 60014618), Textile Research and Technology Institute (TRTI), Pre-treatment and Finishing of Cellulose-based Fibers Department (PFCFD), El-Behouth St. (former El-Tahrir str.), Dokki, P.O. 12622, Giza, Egypt



CrossMark

Abstract

This study explores the use of rice straw-derived cellulose nanofibers (CNFs) for the adsorption of Reactive Black 5 (RB5) and Methylene Blue (MB) dyes from aqueous solutions. Rice straw was treated and mechanically processed to produce CNFs, which were characterized using techniques like FTIR, XRD, SEM, and TEM. The adsorption performance was evaluated under various conditions, including pH, contact time, initial dye concentration, and adsorbent dosage. The results showed high adsorption capacities for both dyes, with maximum capacities of X mg/g and Y mg/g, respectively. The CNFs demonstrated good reusability, maintaining over 99% of their adsorption capacity after multiple cycles. The study aims to develop nanofibers from rice straw that are more efficient and sustainable for the removal of synthetic dyes from wastewater. The lignocellulosic composition of rice straw showed 79.33% α -cellulose and 15.6% lignin, with pretreatment reducing lignin content by 94.68%. The next step was to extract the cellulose and spin it into nanofibers, producing uniform and fine fibers with improved shape with chitosan. The nanofibers were found to be effective in removing the dyes, with accurate adsorption mechanisms and favorable conditions, particularly with increased chitosan content.

Keywords: rice straw, cellulose, electrospinning, adsorption Kinetic study, dye removal.

1. Introduction

This study investigated the possibility of using cellulose extracted from rice straw that is considered natural waste and conversion to cellulose nanofibers (CNFs) as an intelligent system to treat industrial wastewater polluted by dyes and heavy metals. As a result, this study opens the door for rice straws to be used in value-added ways in place of the present damaging methods to the environment.

Cellulosic fibers are mostly found in wood, but they can also be found in considerable amounts in annual plants like wheat, rice, cotton, sisal, jute, and so on. The survival of the ecosystem and ecological concerns are the main drivers behind the increased use of these plants, aside from financial savings. The most significant benefits of cellulosic fibers are their availability, environmental friendliness, biocompatibility, minimal abrasiveness, and high specific stiffness and modulus. [1-11]

To achieve Sustainable Development Goals (SDG) it has Our objectives in this study are double-edged goals is get rid of natural solid waste like rice straw plus produce new useful products (CNFs) used to remove pollutants from industrial wastewater EX (Dyes and Heavy metals). Rice straw represents a significant portion of the global population, particularly in Asia and Africa, rice is a staple diet. However, the yearly cultivation of rice produces enormous amounts of husks (estimated as $\sim 8 \times 10^{11}$ kg) and straw ($\sim 1.5 \times 10^{11}$ kg) Presently, approximately twenty percent of rice straw is put to use in practical ways, like making paper, fertilizers, animal feed, and biofuels and the majority are either burned in place, [12] which leads to polluted the ecological system with increase percent of greenhouse gases (GHG) and increase climate change.

Environmental contaminants that pollute industrial wastewater like (heavy metals -dyes) harm human health in numerous ways and degrade water quality, which upsets the environment.

Heavy metals (HMs) are hazardous and classified as persistent toxic environmental pollutants that are non-degradable and continue in the human food chain which is transferred through fish and they pose serious dangers to both

* Corresponding author: aga.hassabo@hotmail.com; (Ahmed G. Hassabo).

Received date 18 February 2025; Revised date 14 March 2025; Accepted date 27 March 2025

DOI: 10.21608/ejchem.2025.361829.11326

©2025 National Information and Documentation Center (NIDOC)

human health and environmental safety. Removing them from industrial wastewater effectively is crucial for maintaining environmental safety, enhancing sustainability, and safeguarding public health. [13].

Because of the release of colored effluents including reactive dyes, the textile sector is one of the main causes of water contamination. Two such dyes well-known for their environmental toxicity and persistence are reactive black 5 and methylene blue. Effective adsorbents are therefore rather important since conventional wastewater treatment techniques are usually insufficient for dye removal. Derived from plentiful agricultural wastes such as rice straw, cellulose nanofibers (CNFs) offer a sustainable and environmentally acceptable dye adsorption solution.

They may have entered the ecosystem naturally or as a result of human activity [14] Certain concentrations of arsenic (As), cadmium (Cd), mercury (Hg), lead (Pb), copper (Cu), chromium (Cr), and zinc (Zn) may be released into surface or groundwater resources by natural processes such volcanic activity, soil erosion, and rock weathering. [15] The majority of heavy metals (HMs) found in surface waterways are caused by chemical spills, improper industrial wastewater discharge, and contaminants from storm runoff [13, 16, 17] in addition to dyes pollutants produced from improper industrial wastewater discharge from the textiles industry. Many industries use dyes, including the paper, textile, plastic, and food industries. [18]

2. Experimental

2.1. Materials

Rice straw was used as the biomass raw material source for the natural lignocellulosic fiber and was gained from our local Egyptian farmers: Shebin- El Kanater – Qaluobia, where it was dried at room temperature to equilibrium moisture content, Sodium hypochlorite as a bleaching agent was acquired from El Nasr Company for Chemicals.

Sodium hydroxide, sodium chlorite, acetic acid & sulfuric acid 72% (w/w), was gained from El Nasr Company for Chemicals. Sodium carbonate, acetic anhydride, Sulphuric acid, sodium citrate, ethyl alcohol, other solvents, and double distilled water were laboratory-grade chemicals. *N, N'*-dimethyl formamide (DMF), Dimethyl sulfoxide (DMSO), Dimethylacetamide (DMAc), and acetone were purchased from Sigma-Aldrich.

The dye used in this study is Reactive Black 5 (RB5). This dye was kindly supplied, by Sigma-Aldrich USA (molecular weight = 991.82 g/mol, C.I. no. = 306452, λ_{\max} = 597 nm). Basic dye 9 (Methylene Blue) ($C_{16}H_{18}ClN_3S$) was purchased from Carl Roth GmbH Co. Both dyes were used as received and the chemical structure is shown in **Figure 1**.

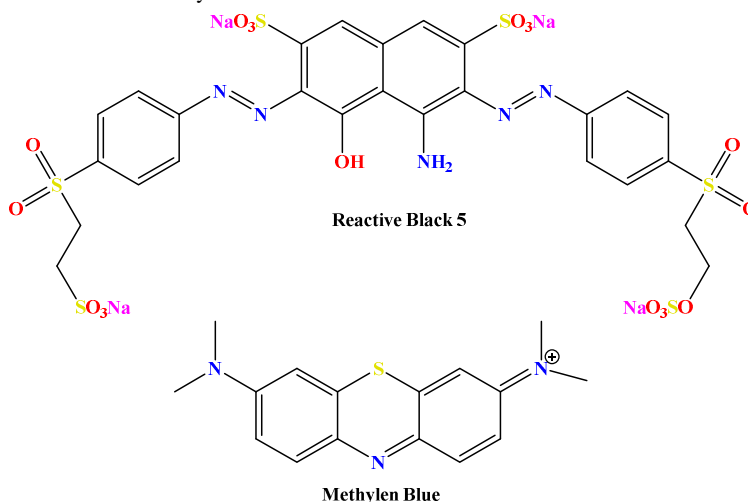


Figure 1: Chemical structure of both used dyes Reactive Black 5 (RB5) Methylene Blue (MB)

2.2. Methods

2.1.1. manufacture Process

2.1.1.1. Alkaline pulping

Rice straw was cut into small pieces, it was added into a pressurized vessel (autoclave) having a solution of 5%wt Sodium hydroxide with liquor solid ratio 10:1, temperature reached 105°C & pressure to the sample reached 15atm, Rice straw was soaked in the autoclave for 2hrs to separate into cellulose fibers and lignin. Cellulose fibers are sent for washing in warm water and then bleach process. [46]

2.1.1.2. Bleaching process

After the cooking process, the fibers are brownish, as they still contain some lignin, which negatively affects the degree of whiteness. High brightness can be obtained by removing the remaining lignin with a bleaching agent. Two methods are used in the bleaching process. The bleaching agent is Sodium hypochlorite NaOCl.

2.1.1.3. Bleaching method

The process which uses sodium chlorite 5% (w/v) was carried on pressure 1atm and room temperature by solid liquor ratio 1:10.

2.1.2. Electrospinning of Cellulose fiber

Produced Cellulose powder from rice straw 2 g was solubilized in a different solvent such as Chloroform, *N, N'*-dimethyl formamide (DMF), Ac/DMAc (2:1) using 10 % ratio for 3 hr, a by vigorous stirring for more 2 hr. Syringe glass 10 ml filled with prepared solutions and connected with the positive part of Electrospinning, the negative part connected to the rotated collector as appeared below. The syringe pump worked at a speed rate of 6 ml/hr. The prepared electro-spun fibers collected and cute for the characterizations [22]. After that chitosan was mixed with cellulose solution (10 %) by three different ratios 1, 2, and 3 %, and then applied to the electrospinning process by the previous condition.

2.2. Analysis and measurements

2.2.1. Rice Straw Chemical Composition Estimation

2.2.1.1. Water absorption

To investigate water absorption, 35 grams of rice straw was dried in an oven at a temperature of 105°C for a period of 2 days to ensure complete evaporation of water, [19, 20] The dried particles were then submerged in water for varying durations ranging from 5 minutes to 48 hours. By observing the absorption rates of the rice straw, denoted as A(t), we can determine the water absorption.

$$A_t = 100 \times \frac{m_t - m_0}{m_0}$$

A_t: water absorption percent, m_t: weight after drying, and m₀: weight before drying

2.2.1.2. Estimation of the Ash present

The ash was estimated from rice straw by ignition [45] where rice straw was cut into small pieces. A weighted material (about 1 g) was ignited in a muffle furnace in a porcelain crucible first at 400 °C for 30 min and then at 850 °C for 45 min and then ash was gravimetrically estimated. The ash percentage was calculated from equation (1).

$$\text{Ash\%} = \frac{\text{weight of ash}}{\text{weight of dry sample}} \times 100 \text{ Equation (1) calculation of Ash percentage}$$

2.2.1.3. Estimation of Lignin

Lignin in raw material was estimated in which, about one gram (exactly weighed) was treated with 72 % sulphuric acid (w/w) with a 20:1 liquor ratio for 4 hours at room temperature about 25-30°C then diluted to 3 % sulphuric acid and boiled for four hours under reflux. The lignin was filtered on an ashless filter paper and washed with hot distilled water till neutrality then gravimetrically estimated and ignited at 400°C for 30 min, then at 800°C for 45 min (1). The weight of ash was subtracted to give the lignin-free ash by using equation (2). [45]

$$\text{Lignin\%} = \frac{\text{weight of lignin} - \text{weight of its ash}}{\text{weight of the dry sample}} \times 100 \text{ Equation (2)}$$

2.2.1.4. Estimation of α -Cellulose and Hemicelluloses:

To determine α -cellulose in the raw material hollo cellulose must be estimated first and from it α -cellulose could be determined. Hollo cellulose was prepared according to the sodium chlorite (NaClO₂) method as follows: Exactly weighed about 5 g of Exacted rice straw was added to 80 ml of distilled water at 75°C, solution must be stirred mechanically, then added acetic acid (0.8 ml) and sodium chlorite (1.86 g) and the reaction was allowed to proceed with vigorous stirring. This process was repeated until the lignin color nearly disappeared. At the end of the response, the remaining hollo cellulose was washed with distilled water until free from acid, acetone, and ether. The product was dried under vacuum at 50°C and then weighed the hollo cellulose. [45]

α -cellulose was determined by using 17.5 % (w/w) sodium hydroxide as follows: About 3 g (exactly weighed) of hollo cellulose was treated first with 25 ml of sodium hydroxide (17.5 % w/w) then left to swell for 4 min at 20°C, the sample was pressed for 3 min with a glass rod, then another 25 ml of NaOH was added and the contents were mixed for 1 min then left covered at 20°C. After 35 min, 100 ml of distilled water was added, followed by filtration in a sintered glass funnel. 100 ml of 10 % acetic acid was drop wisely added for washing followed by distilled water. The α -cellulose percentage was estimated gravimetrically after dryness in a drying oven at 105 °C and after subtracting the ash from Equation (3). [45]

$$\alpha - \text{cellulose\%} = \frac{\text{weight of } \alpha - \text{cellulose} - \text{weight of its ash}}{\text{weight of original hollocellulose sample}} \times 100$$

$$\text{hemicellulose\%} = (\text{hollocellulose\%} - \alpha \text{ cellulose\%}) \text{ Equation (3)}$$

2.2.2. Characterization of produced electro-spun fibers

Electro-spun cellulose fiber homogeneity and fiber diameter were examined through a scanning electron microscope (SEM). Microscopic investigations on electro-spun fibers were carried out using a Philips XL30 scanning electron

microscope (SEM). Images were taken using secondary electrons (SE) by the clarity of the images [23]. Samples were fixed with carbon glue and metalized by gold vapor deposition to record images. The conductivities, viscosity, and surface tension of spinning solutions were measured with a digital conductivity meter (DDS-307A) and NDJ-79 Digital Brookfield viscometer. To achieve that, the conductive electrode was soaked into the solution completely at room temperature, and then the stabilized readings were recorded.

2.2.3. Adsorption and Isothermal Studies

To convert the absorbance measured into concentration and monitor the amount of RB5 and MB adsorbed, five known concentrations for each dye were prepared and measured using 5 cm quartz cells housed in a UV/visible spectrophotometer (UV-1601 Shimadzu, Japan) at λ_{\max} = 597 and 610 nm respectively. This calibration standard curve was established as shown in **Figure 2**

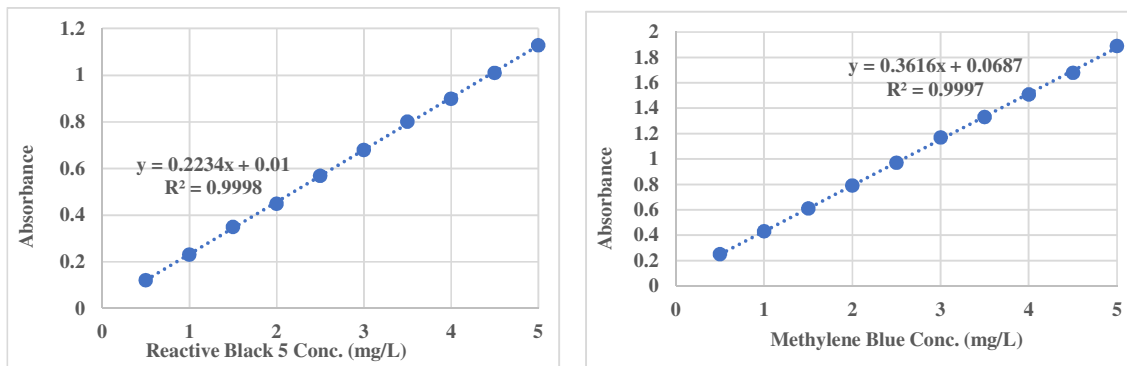


Figure 2: calibration standard curve for both used dyes RB5 and MB

The batch adsorption studies were conducted in Erlenmeyer flasks that contained 100 ml of the dye solution with a concentration of 10-300 mg/L. 2 g of the natural network nanofibre was further added to the samples. The flasks were shaken on a horizontal shaker at a constant speed of 400 rpm and a temperature of 30°C. Subsequently, equilibrium was achieved by stirring the Erlenmeyer flasks for three hours. The UV/visible spectrophotometer (UV-1601 Shimadzu, Japan) was employed to detect the concentration of both dyes RB5 and MB in the solution following equilibrium adsorption at λ_{\max} = 597 and 610 nm respectively. All adsorption experiments were conducted in duplicate, and the mean values were reported.

For kinetic experiments, after the treatment, sampling was done at varied times (10–120 min). 5 ml of the sampled aqueous phase was tested for the residual concentration of both dyes RB5 and MB using a UV-Vis spectrophotometer and then added back into the treatment solution to keep the concentration constant.

For isotherm investigations, 100 ml of the solutions of varied RB5 and MB concentrations (10 – 300 mg/L) were produced in separate 250 ml conical flasks. 1g of nanofibre was placed into each of the conical flasks. After 30 min, the solution was tested then the absorbance was converted to concentration. Duplicate tests were done in parallel to check the results.

2.2.4. Error analysis

In light of the innate predisposition coming about because of the linearization of the isotherm and dynamic models, four different error functions of the non-linear relapse bowl were utilized as criteria for the nature of fitting. [21-23]

2.2.4.1. The root means square error (RMSE)

The root means square test (RMSE) has been utilized by various analysts in the field to test the sufficiency and precision of the model fit with the exploratory information:

$$RMSE = \sqrt{\frac{1}{n-2} \sum_{i=1}^n (q_i - q_{i,e})^2}$$

Where q_i is the test sorption limit from the batch analysis i , $q_{i,e}$ is the sorption capacity evaluated from the sorption model for comparing q_i and n is the number of perceptions in the batch experimental.

2.2.4.2. The chi-squared test (χ^2)

The chi-squared test (χ^2) statistic is the whole sum of the squares of the differences between the experimental data acquired by evaluation from models, with each squared difference divided by the corresponding data obtained by calculating from models. The chi-squared test has some comparability with the root mean square error and is given as:

$$\chi^2 = \sum_{i=1}^n \frac{(q_i - q_{i,e})^2}{q_{i,e}}$$

2.2.4.3. The sum of absolute errors (SAE)

The aggregate of total errors (SAE) is given as:

$$SAE = \sum_{i=1}^n |q_i - q_{i,e}|$$

The isotherm parameters controlled using this method provide a better fit as the size of the errors increments, biasing the fit toward the high-concentration data

2.2.4.4. The average relative error (ARE)

The average relative error (ARE) is characterized as:

$$ARE = \frac{100}{n} \sum_{i=1}^n \left| \frac{q_t - q_{i,e}}{q_t} \right|$$

This error function endeavors to limit the fractional error conveyance over the whole concentration range.

3. Result and Discussion

3.1. Characterization of rice straw

The lignocellulose breakdown efficiency after the chemical composition analysis of rice straw is shown in **Table 1**. The unprocessed rice straw used in this investigation consisted of 79.33% α -cellulose, and 15.6% lignin. Rice straw underwent degradation shortly after undergoing pretreatment. **Table 1** and

Table 2 show that cellulose and lignin's breakdown efficiency was higher than lignin's. Following the pretreatment process, 94.68 % of the lignin was eliminated, with a loss of 39.46 % of cellulose and 6.63 % of ash content. Following processing, the rice straw's structure was significantly damaged, resulting in many fractures.

Bio-based materials possess a notable degree of absorbency as a result of the existence of polysaccharide molecules, namely hemicellulose, and cellulose, which possess the capacity to bind and hold water molecules. To properly employ these materials, it is essential to comprehend their water absorption capability and the speed at which they absorb water. **Table 1** shows the proximate analysis classifies rice straw in terms of its moisture (M), volatile matter (V), fixed carbon (FC), and ash content (A). In addition, yield percent, α cellulose, lignin, and Ash content in rice straw, after pulping with NaOH and after bleaching were reported in

Table 2. Rice straw pulping and bleaching could be successfully performed in NaOH at pressure where the pulp and bleaching obtained has low lignin content, low ash content, and bright white color of cellulose

Table 1: α cellulose%, lignin% moisture content, volatile matter, Ash content, and fixed carbon in rice straw, after pulping and bleaching with NaOH

MATERIAL	rice straw	pulp NaOH	bleaching with NaClO ₂
moisture content (%)	7.20	6.40	7.00
volatile matter (%)	56.90	75.70	68.00
Ash content (%)	27.20	11.20	1.127
fixed carbon (%)	8.70	6.70	8.00
α -cellulose (%)	79.33%	66.66%	79.00%
lignin (%)	15.62%	8.98%	11.57%

Table 2: yield percent, α cellulose, lignin, and Ash content in rice straw, after pulping with NaOH and after bleaching.

Material	yield%	α cellulose%	Lignin%	Ash content%
Rice straw	100%	79.33%	15.60%	27.20%
pulp NaOH	59.20%	39.46%	5.32%	6.63%
NaClO ₂ bleaching	90.28%	31.17%	0.615%	1.127%

FT-IR was used as an analytical instrument to ascertain the chemical structural alterations of rice straw after the bleaching process. The FT-IR spectra of the samples are shown in Figure 3. The analysis focused on measuring the alterations in functional groups of the bleached rice straw within the range of 500 to 4000 cm⁻¹. In the FT-IR spectrum of bleached rice straw. The broad hydroxyl band observed between 3000-3500 cm⁻¹ in all samples indicates the presence of O-H groups in holocellulose, which includes both cellulose and hemicellulose. Additionally, the peaks at 1158 and 1026 cm⁻¹ are associated with the C-O-C stretching in cellulose and hemicellulose. The peaks at 2918 and 1370 cm⁻¹ represent the C-H bonds found in the methyl and phenolic groups of lignin and hemicellulose. The peak at 789 cm⁻¹ signifies the

glycosidic β (1–4) linkage characteristic of cellulose. The peak at 1735 cm^{-1} corresponds to the C=O stretching of the acetyl group present in hemicellulose and lignin, while the band at 1640 cm^{-1} indicates aromatic skeleton stretching.

In the extracted cellulose sample, the absence of peaks at 1740 cm^{-1} and 1242 cm^{-1} , which are associated with carbonyl and aromatic groups in lignin, suggests that effective delignification occurred during the pulping and bleaching processes. However, a slight shoulder at 1740 cm^{-1} remains, indicating the presence of some residual hemicellulose or lignin.

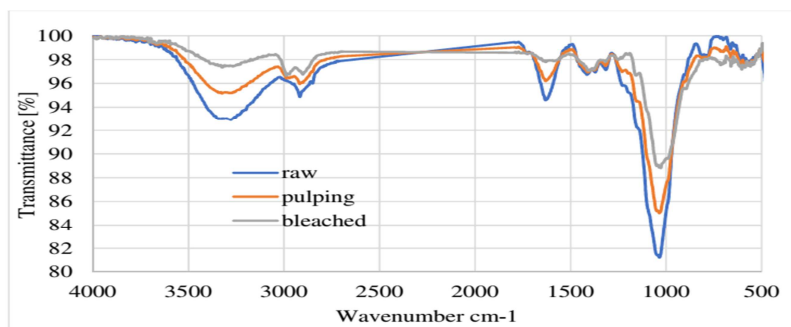


Figure 3: FT-IR spectra of raw and pretreated rice straw

The crystallinity of raw and bleached rice straw. The main purpose of pretreatment is not only to remove lignin but also to break the inter- and intra-chain hydrogen bonding of cellulose fibrils and destroy the cellulose crystalline structure in rice straw, [24] thus making the feedstock more accessible to a broad range of microorganisms. To investigate the crystallinity changes of rice straw after pretreatment, X-ray diffraction (XRD) was performed and the XRD patterns of the raw and pretreated rice straw are shown in Figure 4. The raw rice straw (a) shows lower peak intensities, indicating a lower degree of crystallinity. This is typical for lignocellulosic biomass, which contains amorphous components lignin and hemicellulose. The extracted cellulose (b) exhibits sharper and more intense peaks, particularly around $2\theta = 22^\circ$, which is characteristic of cellulose, the crystalline form of cellulose. This indicates that the Bleaching process effectively removed amorphous components lignin and hemicellulose, enriching the crystalline cellulose content. The XRD spectra demonstrate that bleaching significantly alters the structural composition of rice straw, increasing its crystallinity by removing amorphous lignin and hemicellulose. This change improves the material's suitability for industrial and biochemical applications.

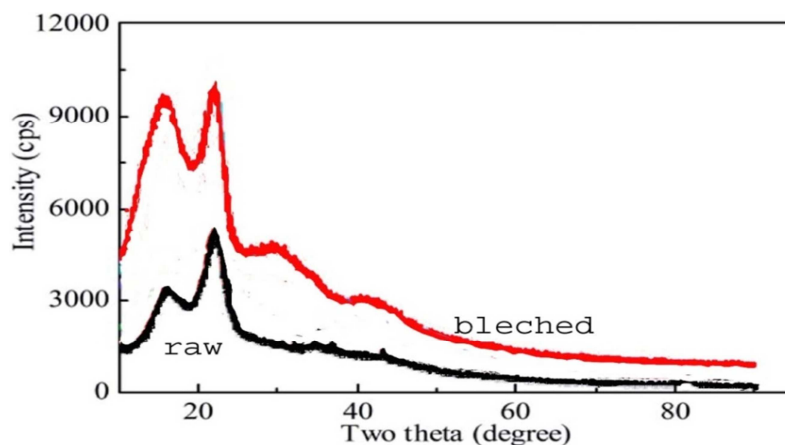


Figure 4: X-ray diffraction spectra; (a) rice straw (b) extracted cellulose

3.2. Characterization of manufactured nanofibers

Ultrafine fibers can be generated from polymer solutions through electrospinning. [25-29] This method can efficiently produce fibers with diameters in the micrometer range of nanometers. The electrospinning process for fiber formation from polymer solutions is significantly influenced by the properties of the solution, including viscosity, surface tension, and net charge density.

In the electrospinning of extracted cellulose solutions, viscosities ranging from 1 to 20 poise and surface tensions between 35 and 55 dynes/cm were appropriate for fiber formation.

Electrospinning was impeded at viscosities exceeding 20 poise due to flow instability resulting from the solution's high cohesiveness. Droplets formed when the viscosity was insufficient (1 poise). Altering the surface tensions of cellulose solutions through modifications in solvent systems has been demonstrated to affect fiber morphology. Understanding solvent systems is crucial for regulating solution properties in the electrospinning process to produce ultrafine fibers.

Electrospun fibers can be engineered to create various structures by employing solvents with elevated vapor pressure or by intentionally incorporating salt into the polymer solution, which is subsequently leached out after drying the

fibers. The resultant structure of electrospun fibers possesses a high surface-to-volume ratio, rendering them suitable for filtration, odor absorption, and diverse smart textile applications. [30-32]

The optimal conditions for spinning extracted cellulose from rice straw waste using various solvents (chloroform, dimethylformamide, AC/DMAC 2:1) were a flow rate of 6 mL/hr, a nozzle-holder distance of 10 cm, and an applied voltage of 20 kV, to examine the influence of different solvents on fiber morphology. The parameters of viscosity, conductivity, and surface tension of the extracted cellulose from rice straw waste solutions were analyzed and presented in

Table 3. Altering the solvent resulted in modifications to the properties of the polymer solution, including conductivity and surface tension. This may contribute to an increase in the polarity of the extracted cellulose solution. SEM images of extracted cellulose electrospun fibers are depicted in figure 5. The electrospinning of cellulose extracted from each solvent produced a broad and uniform spun sheet. The homogeneity was ascribed to a fully soluble solution and uniform distribution resulting from the consistent influence of the electric field on the spun solution from the needle to the collector. Moreover, employing DMF as a solvent resulted in a dense, centrally located bundle sheet.

Table 3 illustrates that the thick fibers, resulting from phase separation, were produced using DMF followed by chloroform, while the combination of acetic acid and dimethylacetamide as a solvent yielded thinner fiber diameters.

From this investigation, it concluded that, using AC/DMAC (2:1) as a solvent the produced nanofiber shows the smaller diameter and the the best homogeneous distributed fiber. Therefore, further investigation occurred to investigate the effect of blending chitosan with extracted cellulose using AC/DMAC as a solvent on the behavior of the produced nano-fibre.

The surface morphology of the electrospun fibers was frequently examined using SEM, as illustrated in Figure 5. Altering the solvent in the spinning of CA yielded remarkable results. The Ac/DMAC (2:1) solvent demonstrated an effective spinning process resulting in thinner fibers. SEM results indicated that morphology and fiber homogeneity improved as the chitosan polymer blending increased from 1 to 3%. Spinning with a low chitosan concentration (1%) produced homogeneous cylindrical fibers with a diameter of 1.2 μm . The fiber diameter was reduced by elevating chitosan concentration to 3%, achieving a measurement of 1.1 μm .

Subsequently, the chitosan fiber diameter was inversely adjusted. The short duration required to reach the collector is attributed to an increase in time, which adversely affects solvent evaporation, resulting in a reduction in fiber diameter and the production of stable electrospun fibers. The incorporation of chitosan may facilitate the separation of extracted cellulose chains from the solvent, thereby promoting rapid solvent evaporation. Simultaneously, hydrogen bonding among water molecules facilitates chain entanglement, enabling the spinning process.

Finally, it can be concluded that blending chitosan with extracted cellulose enhances the morphological behavior and the fiber diameter.

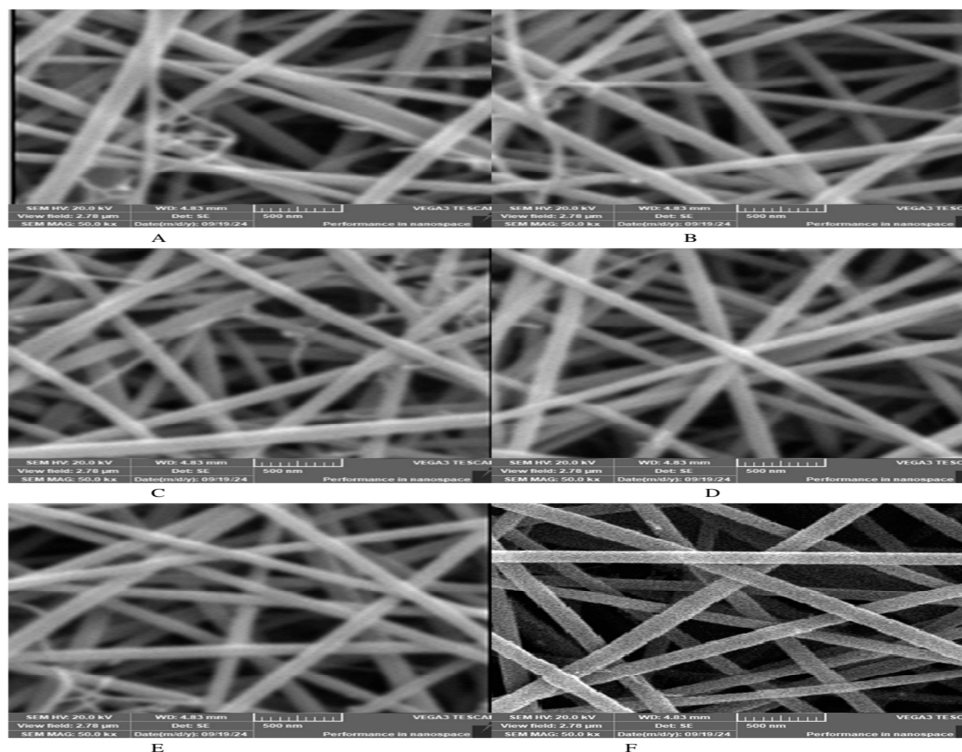


Figure 5: SEM images for produced Electro spun fibers in different solvent A) Cell (10)/DMF, B) Cell (10)/Chloroform, C) Cell (10)/AC/DMAC, D) Cell (10)/Chito (1)/ AC/DMAC, E) Cell (10)/Chito (2)/ AC/DMAC, and F) Cell (10)/Chito (3)/ AC/DMAC.

Table 3: Fiber diameter of electrospun extracted cellulose fibers

Polymer	Solvent	Conductivity $\mu\text{S cm}^{-1}$	Viscosity (mPS s)	Surface tension (Nm m^{-1})	Characteristics	Fiber diameter μm
Cellulose (10%)	Chloroform	5.5	43.25	30.6	Thin fiber	1.9
	Dimethylformamide	7	41.33	39.11	Thick fiber	2.1
	AC/DMAc	4.2	40.11	38.34	Thin fiber	1.3
Cellulose (10%) / Chitosan (1%)	AC/DMAc	4.3	41.22	38.32	Thin fiber	1.2
Cellulose (10%) / Chitosan (2%)	AC/DMAc	4.3	41.32	38.22	Thin fiber	1.1
Cellulose (10%) / Chitosan (3%)	AC/DMAc	4.3	41.44	38.14	Thin fiber	1.1

3.3. Adsorption Study

The nanofibre may engage with RB5 and MB dyes via hydrogen bonding and/or hydrophilic-hydrophobic interactions. This observation may be ascribed to the reduction in dye dissociation, resulting in a diminished concentration of dye species available to engage with the nanofibre active sites. This behavior can be elucidated by the diminished degree of protonation of functional groups, specifically carboxylic groups.

The dye uptake was determined by the difference in dye concentrations in the supernatant, utilizing the following equation:

$$Q = V(C_0 - C_f) / M$$

Q represents the dye uptake (mg/g), C_0 and C_f denote the initial and final dye concentrations in the solution (mg/l), respectively, V signifies the volume of the solution (L), and M indicates the weight of the nanofibre (g).

3.3.1. Effects of the contact time on the adsorption of dye onto nanofiber surface

Figure 6 illustrates the dye Concentration as a function of time at an initial dye concentration of 40 mg, efficiency of dye adsorption (%), and Adsorbed Dye Concentration (mg dye/mg fiber) in the uptake of RB5 and MB correspondingly by the nanofibre. Approximately 95% of the overall absorption of RB5 was attained within 60 minutes.

3.4. Kinetic Study

The kinetics of the adsorption processes provide useful information regarding the efficiency of adsorption and the feasibility of scale-up operations. The concentration-time curves (**Error! Reference source not found.**) of the adsorption of RB5 and MB on the surface of nanofibers suggest that both dyes (RB5 and MB) adsorb on the prepared nanofibers very well, exhausting about 95% from dye bath effluent. [3, 8, 33-37]

Three kinetic models were tested to find out the appropriate expression for the adsorption rate, viz.: the pseudo-first-order [38], the pseudo-second-order model [39], and the Intra-particle diffusion model [40]. The pseudo-first-order rate equation is given below:

$$\frac{dq}{dt} = k_1(q_e - q_t)^n$$

Where q_t is the amount of dye adsorbed (mg/g) at time t , q_e is the maximum adsorption capacity (mg/g), k is the rate constant (min) and n is the reaction order. On integration, the linear form can be written:

$$\ln(q_e - q_t) = \ln(q_e) - k_1 t \text{ For } n=1 \text{ (first-order reaction)}$$

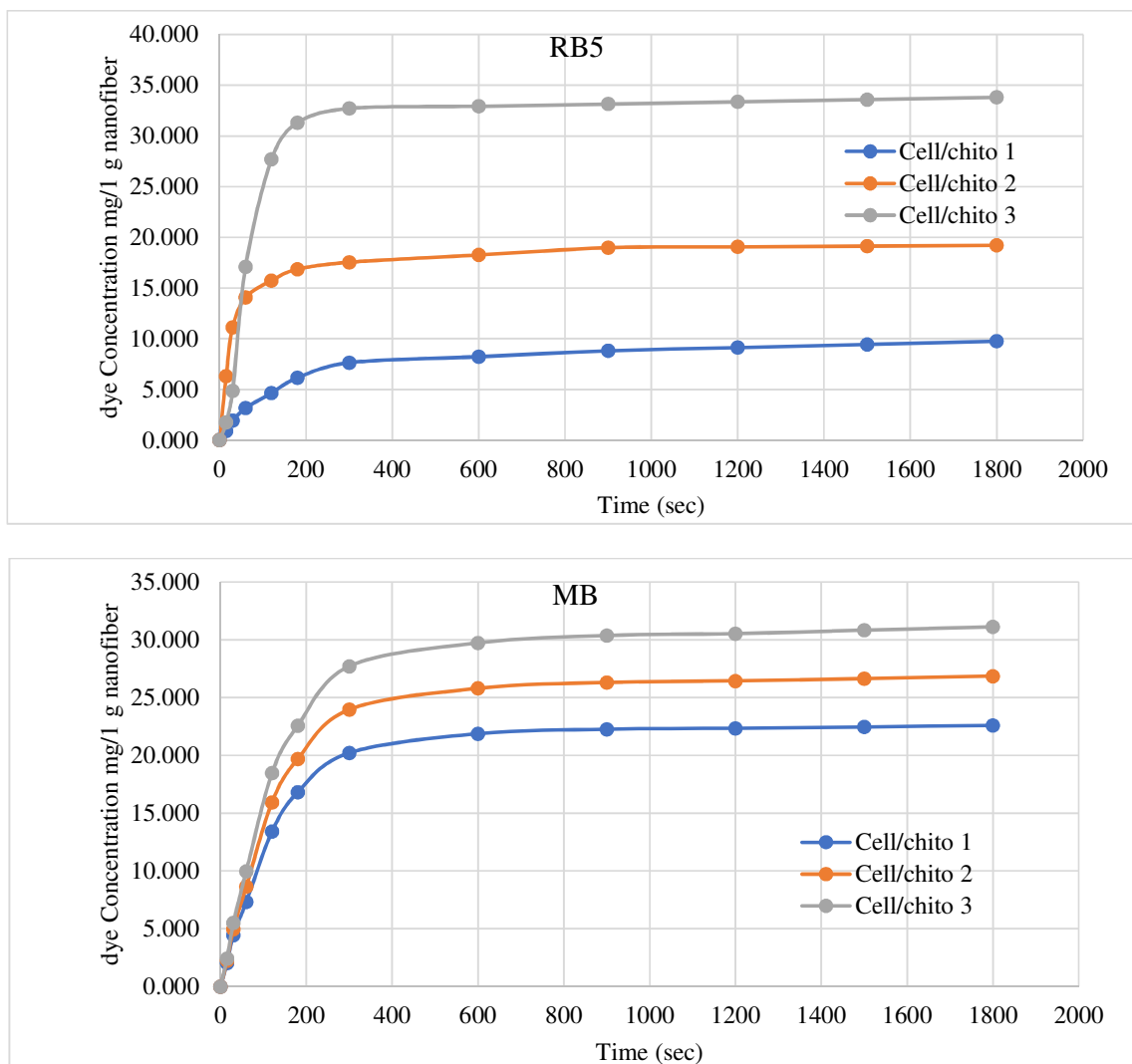


Figure 6: the concentration-time curve of RB5 and MB onto the surface of nanofibre at 25°C

The rate of the pseudo-second-order model depends on the amount of dye adsorbed on the surface of the adsorbent and the quantity adsorbed at equilibrium [41]. After integration, the model was written as:

$$\frac{1}{q_t} = \left(\frac{1}{k_2 q_e^2} \right) \left(\frac{1}{t} \right) + \frac{1}{q_e}$$

Where q_t is the amount of dye adsorbed (mg/g) at time t , q_e is the maximum adsorption capacity (mg/g) for second-order adsorption, and k_2 is the second-order rate constant (g/mg.min).

Both of pseudo first and pseudo second order models above cannot be used only to identify the diffusion mechanism, so the intra-particle diffusion model was proposed. The initial rate of the intra-particle equation is the following [40]:

$$Q_t = K_d t^{1/2} + C$$

Where k_d is the intra-particle rate constant (g/mg min^{-1/2}), and it is a function of equilibrium concentration in the solid phase, Q_t and intra-particle diffusion C can be determined.

From the above equations, the values of the adsorption rate constant (k) for RB5 and MB adsorption on nanofiber were determined. In addition, the values of other parameters and the correlation coefficient were calculated for each plot.

The value of reaction order was chosen for which the best linear correlation is achieved (the highest value for R^2). The corresponding values of rate-constant (k) and correlation coefficients R_1^2 are given in Table 4. The results in **Error! Reference source not found.** indicate that the best fit is given by a pseudo-second-order kinetics model for the data of adsorption of RB5 by each prepared nanofiber. The pseudo-second-order kinetic model suggests also that the mechanism of adsorption is a diffusional one via micropores (figures are omitted). In addition, The results in Table 4 indicate that the best fit is given by a pseudo-first-order kinetics model for the data of adsorption of MB by each prepared nanofiber. The pseudo-first-order kinetic model suggests also that the mechanism of adsorption is a diffusional one via micropores (figures are omitted).

However, the plot of RB5 and MB uptake Q_t versus square root of time $t^{1/2}$ does not pass through the origin in this study (**Figure 7** and **Figure 8**). This indicates that intraparticle diffusion in the sorption process is not the only rate-limiting step but also other kinetic processes may be occurring and contribute to the sorption mechanism [40].

Table 4: The kinetic parameters values as obtained from the experimental data for both dyes using different nanofibres

Nanofiber	Parameters	RB5			MB		
		Pseudo First-order model	Pseudo Second-order model	Intraparticle diffusion model	Pseudo First-order model	Pseudo Second-order model	Intraparticle diffusion model
Cell/chito 1	R^2	0.854	0.9816	0.858	0.9993	0.9918	0.7539
	K	0.005067	0.0007	0.2132	0.0076	0.0003	0.4946
	C			1.9016			5.6827
	Q_e	9.3154	8.5985		22.9879	20.0401	
Cell/chito 2	R^2	0.854	0.9998	0.6467	0.9994	0.9949	0.7564
	K	0.0076	0.0021	0.2372	0.0076	0.0004	0.5912
	C			11.081			6.5525
	Q_e	11.7247	19.4175		27.4410	28.4900	
Cell/chito 3	R^2	0.9704	0.984	0.5704	0.9991	0.9943	0.758
	K	0.012436	0.0003	0.6564	0.00737	0.0003	0.6879
	C			11.987			7.4223
	Q_e	34.4509	35.9712		31.8933	33.1126	

3.5. Isothermal Studies

The maximum sorption capacities at varying initial dye concentrations were assessed using a UV-Vis spectrophotometer, with the results depicted as adsorbed dye concentration (mg/g) or dye adsorption efficiency (%) against different initial dye concentrations, as illustrated in **Figure 9** and **Figure 10**. It is evident from these figures that increasing the dye concentration in the dye bath from 1 to 30 mg/100 ml enhances the maximum adsorbed dye concentration alongside the increment of chitosan in the nanofibers (1 to 3%). Conversely, the calculation of dye adsorption efficiency (%) demonstrates a discernible reversible trend, indicating that the efficiency of dye adsorption diminishes as the dye concentration increases, exhibiting varying values until reaching 10 mg/100 ml, after which further increases in dye concentration lead to a decline in dye efficiency.

The curve of adsorbed dye concentration can also be utilized to characterize the adsorption isotherm, modeling the interaction of nanofibers with both dyes (RB5 and MB). [35, 42] Adsorption isotherms are characterized by many models, with the most commonly utilized for textile fibers being the Langmuir, Freundlich, BET, and Dubinin-Radushkevich models. [35, 42]

The Langmuir isotherm is extensively employed to characterize single-solute systems. [43] This isotherm posits that intermolecular interactions diminish swiftly with distance, hence forecasting monolayer coverage of the dye on the external surface of the nanofibers. The additional assumption is that adsorption takes place at specified homogenous spots on the nanofibers' surface, with negligible interaction among the adsorbed species. The Langmuir isotherm is represented by the subsequent equation:

$$q_e = \frac{q_m C_e K_L}{1 + C_e K_L}$$

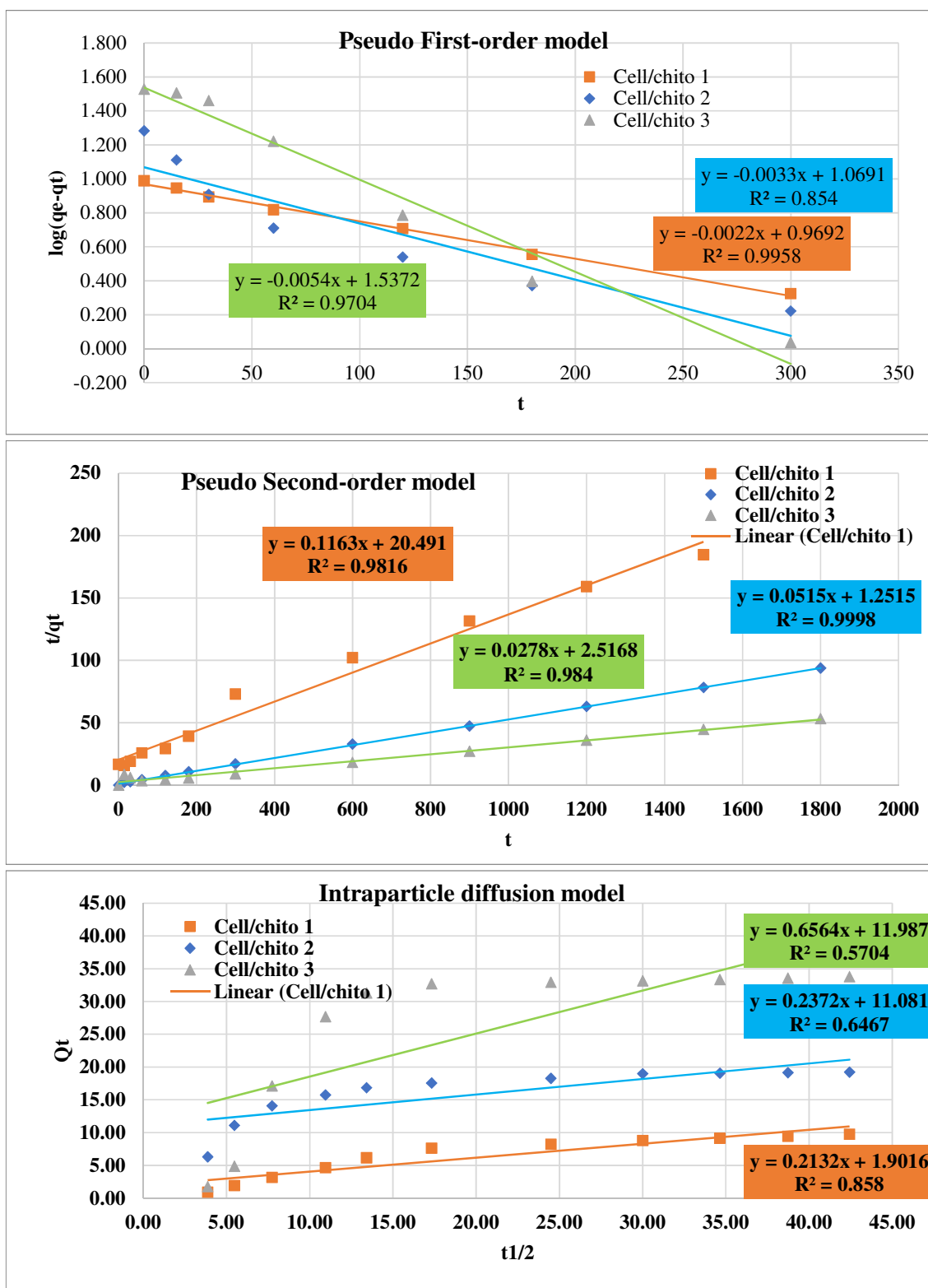


Figure 7: adsorption models of kinetic parameter for RB5 dyes using different nanofibres

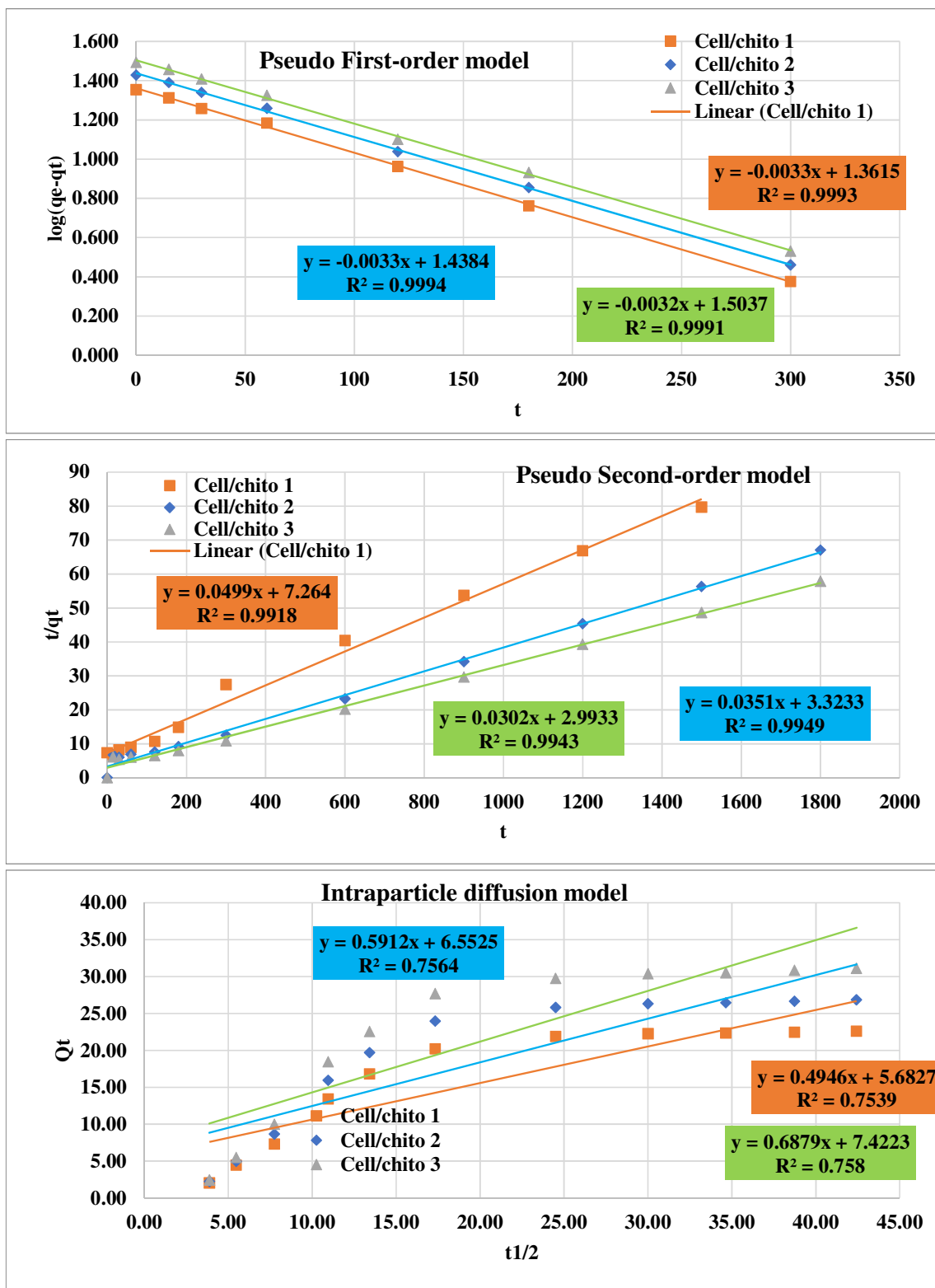


Figure 8: adsorption models of kinetic parameter for MB dyes using different nanofibres

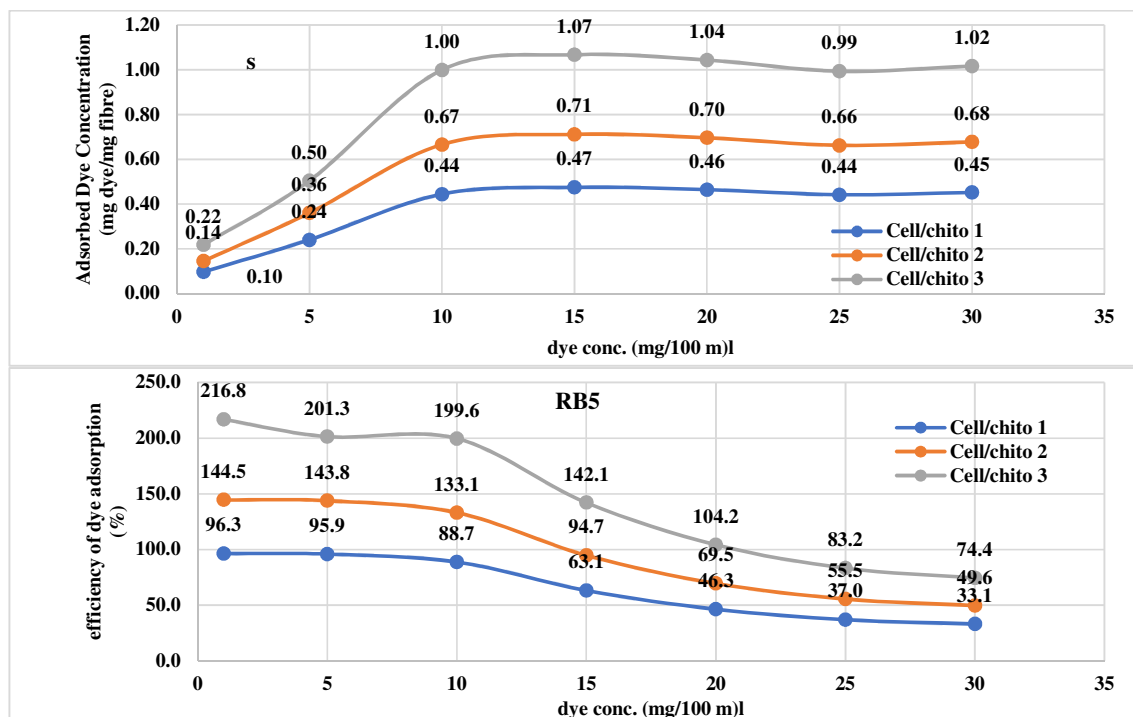


Figure 9: Adsorbed Dye Concentration (a) and efficiency of dye adsorption (%) (b) of RB5 onto the surface of nanofibre

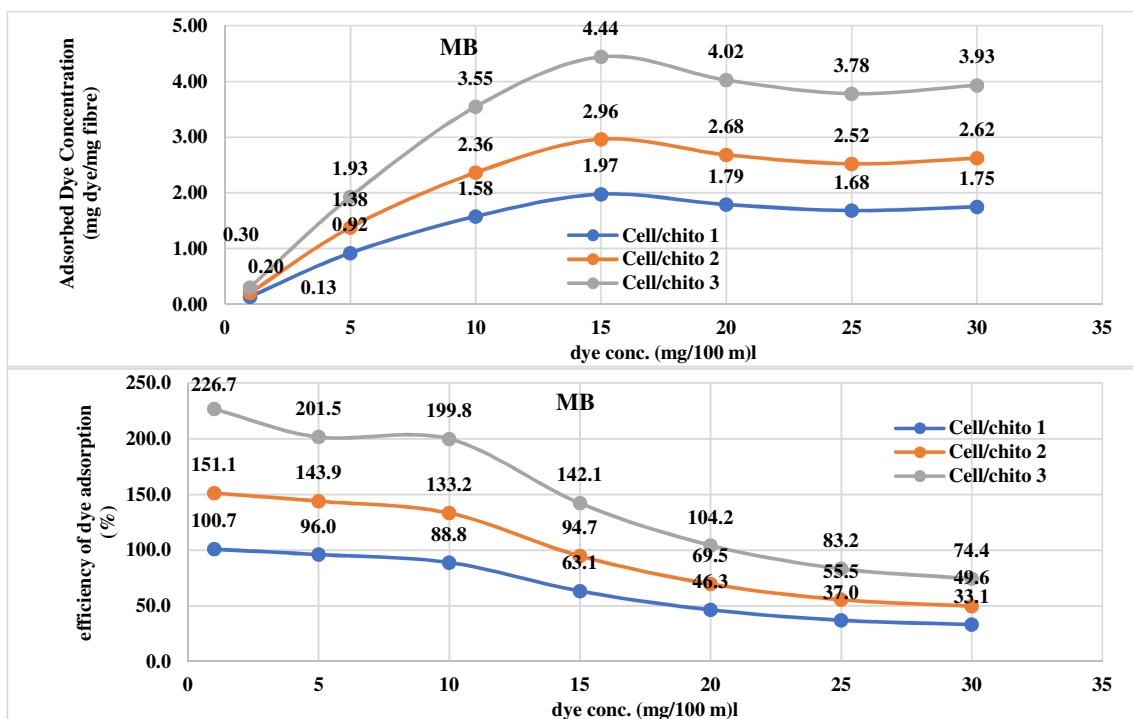


Figure 10: Adsorbed Dye Concentration (a) and efficiency of dye adsorption (%) (b) of MB onto the surface of nanofibre

In this context, q_e represents the equilibrium dye concentration on the nanofibres composite (mg/g), C_e denotes the equilibrium dye concentration in solution (mg/l), q_m indicates the maximum capacity of the nanofibres (mg/g), and K_L refers to the Langmuir adsorption constant (L/mg). By rearranging the components in the aforementioned equation, a line-

ar representation of the Langmuir isotherm can be articulated as demonstrated in the subsequent equation. The graph of $1/q_e$ against $1/C_e$ yields a linear relationship characterized by a slope of $1/q_e K_L$ and an intercept of $1/q_m$.

$$\frac{1}{q_e} = \frac{1}{q_m} + \left(\frac{1}{q_m K_L} \right) \left(\frac{1}{C_e} \right)$$

The Freundlich isotherm effectively characterizes heterogeneous systems. [43] This empirical formula was utilized to investigate the adsorption of dye compounds on the surface of nanofibers. The Freundlich isotherm equation is presented below:

$$q_e = K_F C_e^{1/n}$$

In this context, q_e represents the equilibrium dye concentration on the surface of the nanofibres (mg/g), C_e denotes the equilibrium dye concentration in the solution (mg/l), K_F signifies the Freundlich adsorption constant (L/mg), and n indicates the heterogeneity factor. The linear representation of the Freundlich isotherm is seen in the equation below. The graph of $\ln(q_e)$ against $\ln(C_e)$ produces a linear relationship, characterized by a slope of $1/n$ and an intercept of $\ln(K_F)$.

$$\ln q_e = \ln K_F + \frac{1}{n} \ln C_e$$

The third isotherm model employed in this investigation was the Brunauer-Emmett-Teller (BET) isotherm model. [44] This model was employed to interpret the adsorption data, expressed in its linear form as:

$$C_f = \frac{(K_b - 1)(K_b C_{\max} C_s) + K_b C_{\max} C_i}{(C_i - C_s)(K_b - 1)}$$

In this context, C_f represents the dye concentration adsorbed on the nanofibre composite surface, C_s denotes the dye concentration in the treatment bath, C_{\max} indicates the maximum adsorption capacity of the nanofibres (mg/g), C_i refers to the saturation concentration of dye (mg/l), and K_b is the constant that characterizes the energy of interaction with the nanofibres surface. The linear equation for the Brunauer-Emmett-Teller (BET) isotherm is:

$$\frac{C_s}{(C_i - C_s)C_f} = \frac{1}{K_b C_{\max}} + \left(\frac{K_b - 1}{K_b C_{\max}} \right) \left(\frac{C_s}{C_i} \right)$$

The plot of $(f C_s / (C_i - C_s) C_f)$ versus (C_s / C_i) gives a straight line with the slope of $((K_b - 1) / (K_b \times C_{\max}))$ and the intercept of $(1 / (K_b - 1))$.

Additionally, the experimental results were analyzed using the Dubinin-Radushkevich (D-R) model to ascertain if the adsorption process was physical or chemical in nature. The D-R equation is more comprehensive than the Langmuir model as it does not presuppose a uniform surface, a constant sorption potential, or the lack of steric hindrance between adsorbed and incoming particles. The linear representation of this model is expressed by the following equation.

$$\ln q_e = \ln q_m - \beta \varepsilon^2$$

In this context, q_e (mmol/g) denotes the quantity of dye adsorbent per gram of nanofibers, q_m (mmol/g) signifies the maximum sorption capacity of the adsorbent, β ($\text{mol}^2 \cdot \text{kJ}^{-2}$) is a constant associated with sorption energy, and ε represents the Polanyi sorption potential, which is determined by the subsequent equation:

$$\varepsilon = RT \ln \left(1 + \frac{1}{C_e} \right)$$

In this context, R represents the gas constant, valued at $8.314 \text{ J} \cdot \text{mol}^{-1} \cdot \text{K}^{-1}$, and C_e (M) signifies the dye equilibrium concentration. The Polanyi sorption model posits a constant volume of sorption space next to the sorbent surface and the presence of a sorption potential inside these areas. The sorption space surrounding a solid surface is defined by a series of equipotential surfaces that possess identical sorption potential. The sorption potential is temperature-independent but changes based on the characteristics of the sorbent and sorbate.

The parameters β and q_m were derived from the slope and intercept of the $\ln q_e$ against the ε^2 plot. The mean free energy of sorption E (kJ mol^{-1}) necessary for transferring one mole of dye from infinity in the solution to the surface of nanofibers can be calculated using the following equation:

$$E = (-2\beta)^{-\frac{1}{2}}$$

Every parameter value obtained from the curve fits using the aforementioned four adsorption isotherms are enumerated in. The Dubinin–Radushkevich isotherm is typically utilized to characterize the adsorption mechanism with a Gaussian energy distribution on a heterogeneous surface. The method was often utilized to differentiate between the physical and chemical adsorption of both dyes (RB5 and MB) in their aqueous solutions, using the mean free energy, E , per molecule of adsorbate, which represents the energy required to remove a molecule from its position in the sorption space to infinity. The mean free energy, E values, rose with the concentration of chitosan in the nanofibers for both colors utilized. The E values climbed from 0.98, 1.49, and 2.26 kJ/mol for RB5 dye, and 8.7, 13.87, and 20.41 kJ/mol for MB dye, corresponding to the three examined nanofibers as the chitosan concentration in the nanofiber rose from 1% to 3%, respectively. Denoting a chemo-sorption process (Table 5 and Table 6). [45]

The Langmuir adsorption model demonstrates superior alignment with the experimental data, as indicated by its higher R^2 correlation coefficients compared to other models. Furthermore, the adherence to the Langmuir model indicates that both employed dyes (RB5 and MB) can adsorb onto the active regions of the nanofibers, resulting in monolayer coverage. Moreover, since the n value from the Freundlich model exceeds 1, it indicates favorable adsorption conditions (Figure 11 and Figure 12). [46]

Table 5: Comparison between the parameters of adsorption isotherm models for RB5 on three different nanofibres with chitosan

Nanofiber	Parameter	Langmuir model	Freundlich model	BET model	Dubinin – Radushkevich model
Cell/Chito 1	R^2	0.9876	0.004	0.9536	0.9585
	C_{\max} (mg/g)	0.055224	0.45	-0.70431	4.0002
	K	4.755633	452.0641	-127.019	
	$1/n$		0.0016		
	β				0.5233
	E				0.98
	RMSE	0.409	0.185	1.285	4.294
	X^2	15.158	0.380	-11.725	23.051
	SAE	54.589	53.059	59.905	48.153
ARE	84.457	153.680	298.237	1096.471	
Cell/Chito 2	R^2	0.9876	0.004	0.8743	0.9616
	C_{\max} (mg/g)	0.082836	0.68	-0.76132	1.8855
	K	4.755633	677.6415	-180.329	
	$1/n$		0.0016		
	β				0.2244
	E				1.49
	RMSE	0.379	0.394	1.352	1.796
	X^2	8.685	1.147	-12.007	8.558
	SAE	54.414	52.381	60.304	50.267
ARE	80.308	209.092	314.281	524.379	
Cell/Chito 3	R^2	0.9796	0.004	0.1871	0.9593
	C_{\max} (mg/g)	0.12133	1.02	-2.15312	1.3413
	K	4.640864	1017.1851	-70.7238	
	$1/n$		0.0016		
	β				0.0978
	E				2.26
	RMSE	0.339	0.778	2.994	1.156
	X^2	4.725	2.976	-20.811	4.986
	SAE	54.221	51.364	70.047	50.812
ARE	84.434	292.210	706.019	377.144	

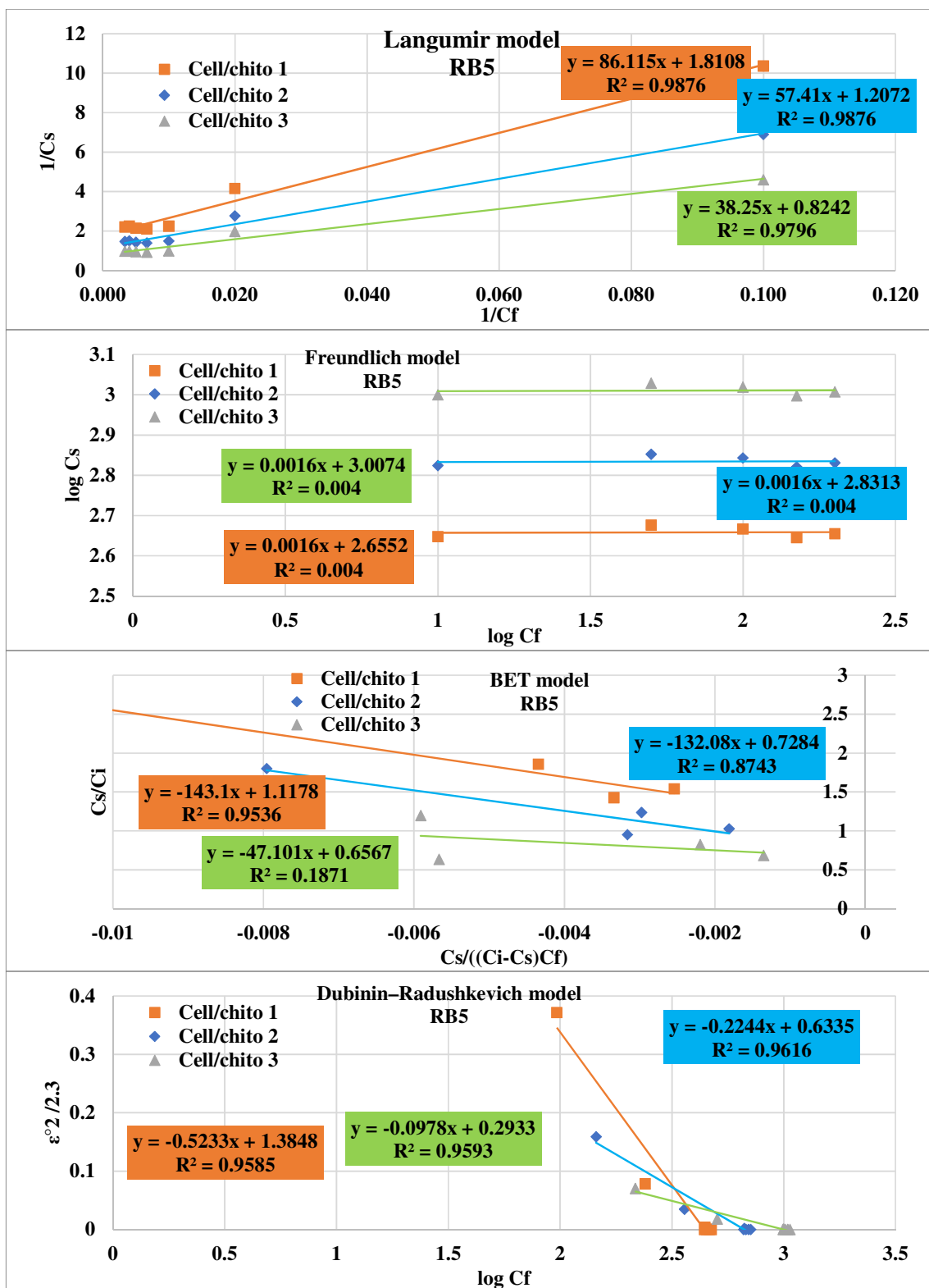


Figure 11: Isothermal models for RB5 dyes using different used nanofibres

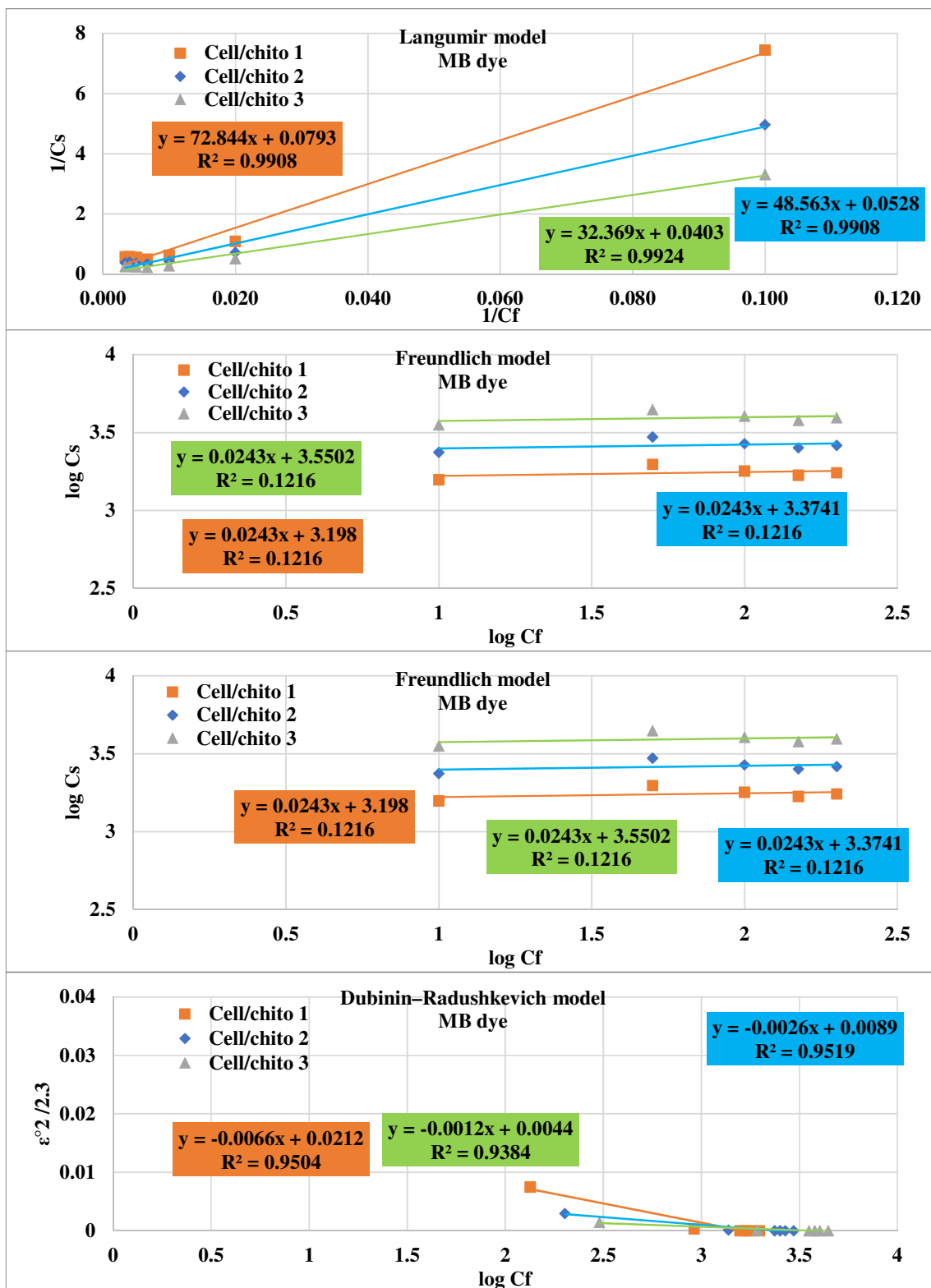


Figure 12: Isothermal models for MB dyes using different nanofibres

Table 6: Comparison between the parameters of adsorption isotherm models for MB on three different nanofibres with chitosan

		Langmuir model	Freundlich model	BET model	Dubinin – Radushkevich model
Cell/Chito 1	R^2	0.9908	0.0216	0.9468	0.9504
	C_{max} (mg/g)	1.261034	1.75	3.152158	1.0215
	K	91.85876	1577.6113	78.66179	
	1/n		0.0243		
	β				0.0066
	E				8.70
	RMSE	0.733	0.822	2.190	0.844
	X^2	2.130	1.933	7.605	3.488
	SAE	206.889	205.430	201.215	207.607
ARE	325.828	434.933	750.188	272.066	
Cell/Chito 2	R^2	0.9908	0.1216	0.9224	0.9519
	C_{max} (mg/g)	1.893939	2.62	-3.61464	1.0089
	K	91.97538	2366.4645	-105.714	
	1/n		0.0243		
	β				0.0026
	E				13.87
	RMSE	0.920	1.608	5.979	0.852
	X^2	2.237	4.936	-49.453	3.599
	SAE	204.990	202.809	237.653	207.645
ARE	467.849	630.971	946.989	269.261	
Cell/Chito 3	R^2	0.9924	0.1216	0.5625	0.9384
	C_{max} (mg/g)	2.48139	3.93	-6.14545	1.0044
	K	80.3201	3549.7682	-94.7159	
	1/n		0.0243		
	β				-0.0012
	E				20.41
	RMSE	1.462	3.076	8.959	0.855
	X^2	4.309	12.033	-65.310	3.640
	SAE	203.228	198.878	255.369	207.658
ARE	599.671	925.028	1540.015	268.244	

4. Conclusion

In this comprehensive study, the characterization and processing of rice straw to manufacture nanofibers were thoroughly explored, with a focus on enhancing adsorption properties for dye removal. The investigation revealed several key findings:

- **Rice Straw Processing:** Through pulping and bleaching using NaOH and NaClO₂, rice straw experienced significant delignification, resulting in a structure with markedly increased absorbency due to reduced lignin and ash content.
- **Crystallinity and Structural Changes:** The pretreated rice straw showed enhanced crystallinity, making it more suitable for microbial interactions. X-ray diffraction confirmed that the bleaching process effectively increased the crystalline cellulose content by removing amorphous lignin and hemicellulose.
- **Nanofiber Formation and Characterization:** Electrospun fibers from rice straw were successfully generated, showcasing varied structural attributes depending on solvent choice. The blending of chitosan with extracted cellulose improved fiber morphology and consistency, leading to more desirable fiber properties for industrial applications.
- **Adsorption Efficiency:** The resultant nanofibers exhibited impressive dye adsorption capacities, notably with both RB5 and MB dyes. The pseudo-second-order kinetic model for RB5 and pseudo-first-order for MB best described the adsorption process, suggesting that surface adsorption plays a crucial role.
- **Isothermal Studies:** Langmuir isotherm models indicated monolayer adsorption on homogeneous sites, while the increase in chitosan concentration in nanofibers correlated with improved adsorption capacity and energy interactions with dyes. In summary, this study demonstrates the potential of rice straw-derived nanofibers as effective adsorbents in textile dye removal. The integration of chitosan enhances structural and functional characteristics, paving the way for sustainable environmental applications in dye pollution mitigation. Future research may further optimize these fibers' performance in real-world scenarios and expand on other potential uses.

5. Conflict of interest

The authors declare that there is no conflict of interest.

6. Declaration section

The datasets used and/or analyzed during the current study are available from the corresponding author upon reasonable request.

7. Acknowledgments

The authors are gratefully grateful to acknowledge the Ain Shams University, Faculty of Graduate Studies and Environmental Research Basic Science Department, Cairo, Egypt. Furthermore, the authors are gratefully grateful to acknowledge the Chemical Engineering Department, National Research Centre Higher Institute of Engineering, El-Shorouk Academy, Cairo, Egypt. Furthermore, the authors are gratefully grateful to acknowledge the Central Labs Services (CLS) and Centre of Excellence for Innovative Textiles Technology (CEITT) in Textile Research and Technology Institute (TRTI), National Research Centre (NRC) for the facilities provided.

8. Reference

- [1]. N. Sharma, B.J. Allardyce, R. Rajkhowa, R. Agrawal, Rice straw-derived cellulose: A comparative study of various pre-treatment technologies and its conversion to nanofibres, *Scientific Reports* 13(1) (2023) 16327.
- [2]. B. Nasri-Nasrabadi, T. Behzad, R. Bagheri, Extraction and characterization of rice straw cellulose nanofibers by an optimized chemomechanical method, *Journal of Applied Polymer Science* 131(7) (2014).
- [3]. M.M. El-Zawahry, F. Abdelghaffar, R.A. Abdelghaffar, A.G. Hassabo, Equilibrium and kinetic models on the adsorption of reactive black 5 from aqueous solution using eichhornia crassipes/chitosan composite, *Carbohydrate Polymers* 136 (2016) 507-515.
- [4]. A.G. Hassabo, A.L. Mohamed, Multiamine modified chitosan for removal metal ions from their aqueous solution *BioTechnology: An Indian Journal* 12(2) (2016) 59-69.
- [5]. E. El-Sayed, H.A. Othman, A.G. Hassabo, Cyclodextrin usage in textile industry, *J. Text. Color. Polym. Sci.* 18(2) (2021) 111-119.
- [6]. A.G. Hassabo, M. Zayed, M. Bakr, E. Abd El-Aziz, H. Othman, Applications of supercritical carbon dioxide in textile finishing: A review, *J. Text. Color. Polym. Sci.* 19(2) (2022) 179-187.
- [7]. E. Abd El-Aziz, R.H. Abd El-Rahman, A.A. Mokhtar, S.S. El-Desoky, G.A. El-Bahrawy, H.A. Ezat, A.G. Hassabo, Textile effluent as a potential problem for environmental and human health: Causes and overcome techniques, *Egy. J. Chem.* 66(12) (2023) 445 - 453.
- [8]. M.M. El-Zawahry, A.G. Hassabo, A.L. Mohamed, Preparation of cellulose gel extracted from rice straw and its application for metal ion removal from aqueous solutions, *Int. J. Biol. Macromol.* 248 (2023) 125940.
- [9]. S.A. Ebrahim, H. Othman, A.G. Hassabo, Enhancing polymer matrix reinforcements: Exploring the potential of biologically modified clay minerals in dyeing, pigment dyes, and wastewater treatment, *J. Text. Color. Polym. Sci.* (2024)
- [10]. L.S. Abd-Elaal, A.N. El-Wekil, A.G. Marey, L.N. Allam, A.G. Hassabo, Supercritical carbon dioxide as an impregnation medium for producing functional materials in textile finishing, *J. Text. Color. Polym. Sci.* 22(1) (2025) 187-195.
- [11]. M.M. El-Zawahry, A.G. Hassabo, F. Abdelghaffar, R.A. Abdelghaffar, O.A. Hakeim, Preparation and use of aqueous solutions magnetic chitosan / nanocellulose aerogels for the sorption of reactive black 5, *Biointerf. Res. Appl. Chem.* 11(4) (2021) 12380 - 12402.
- [12]. B.A. Goodman, Utilization of waste straw and husks from rice production: A review, *Journal of Bioresources and Bioproducts* 5(3) (2020) 143-162.
- [13]. M. Salehi, D. Sharafoddinzadeh, F. Mokhtari, M.S. Esfandarani, S. Karami, Electrospun nanofibers for efficient adsorption of heavy metals from water and wastewater, (2021).
- [14]. Z. Zhaoyong, Y. Xiaodong, Y. Shengtian, Heavy metal pollution assessment, source identification, and health risk evaluation in aibi lake of northwest china, *Environmental monitoring and assessment* 190 (2018) 1-13.
- [15]. L. Qu, H. Huang, F. Xia, Y. Liu, R.A. Dahlgren, M. Zhang, K. Mei, Risk analysis of heavy metal concentration in surface waters across the rural-urban interface of the wen-rui tang river, china, *Environmental pollution* 237 (2018) 639-649.
- [16]. W. Ouyang, Y. Wang, C. Lin, M. He, F. Hao, H. Liu, W. Zhu, Heavy metal loss from agricultural watershed to aquatic system: A scientometrics review, *Science of the Total Environment* 637 (2018) 208-220.
- [17]. K. Aghilinasrollahabadi, M. Salehi, T. Fujiwara, Investigate the influence of microplastics weathering on their heavy metals uptake in stormwater, *Journal of hazardous materials* 408 (2021) 124439.
- [18]. L.A. Mokif, Removal methods of synthetic dyes from industrial wastewater: A review, *Mesopotamia Environmental Journal (mesop. environ. j)* ISSN: 2410-2598 5(1) (2019) 23-40.
- [19]. A. Abakar, A. Dadi Mahamat, A. Donnot, J.-L. Tanguier, R. Benelmir, Physical and chemical characteristics of rice straw, *Research Journal of Applied Sciences, Engineering and Technology* 17(4) (2020) 115-121.
- [20]. T.-T. Nguyen, V. Picandet, S. Amziane, C. Baley, Influence of compactness and hemp hurd characteristics on the mechanical properties of lime and hemp concrete, *European Journal of Environmental and Civil Engineering* 13(9) (2009) 1039-1050.

- [21]. M.N. Sahmoune, K. Louhab, Kinetic analysis of trivalent chromium biosorption by dead streptomyces rimosus biomass, *The Arabian Journal for Science and Engineering* 35(2B) (2010) 69-80.
- [22]. M.N. Sahmoune, K. Louhab, A. Boukhiar, Biosorption of cr (iii) from aqueous solutions using bacterium biomass streptomyces rimosus, *International Journal of Environmental Research* 3(2) (2009) 229-238.
- [23]. K.L. Wasewar, M. Atif, B. Prasad, I.M. Mishra, Adsorption of zinc using tea factory waste: Kinetics, equilibrium and thermodynamics, *CLEAN – Soil, Air, Water* 36(3) (2008) 320-329.
- [24]. T. Sheng, L. Zhao, L. Gao, W. Liu, G. Wu, J. Wu, A. Wang, Enhanced biohydrogen production from nutrient-free anaerobic fermentation medium with edible fungal pretreated rice straw, *RSC Adv* 8(41) (2018) 22924-22930.
- [25]. H. Liu, Y.L. Hsieh, Ultrafine fibrous cellulose membranes from electrospinning of cellulose acetate, *Journal of Polymer Science Part B: Polymer Physics* 40(18) (2002) 2119-2129.
- [26]. H. Othman, E.A. Awad, S.A. Zaher, L.T. Mohamed, E.A. Dabour, E.S. Youssif, M.A. Almouregi, A.G. Hassabo, Electrospinning process parameters and application: A review, *J. Text. Color. Polym. Sci.* 22(1) (2025) 59-66.
- [27]. A.L. Mohamed, A.G. Hassabo, A.A. Nada, S. Zaghlool, Encapsulation of nicotinamide into cellulose based electrospun fibres, *JAPS* 6(8) (2016) 13-21.
- [28]. A.A. Nada, R.A. Abd El-Azeem, A.G. Hassabo, A.L. Mohamed, H.M. Ibrahim, W. Fayad, N.Y. Abou-Zeid, Encapsulation of ricinoleic acid into electrospun ethyl cellulose fibers, 11th International Conference on Nanosciences & Nanotechnologies – NN14, Porto Palace Conference Centre & Hotel, Thessaloniki, Greece, 2014.
- [29]. A.G. Hassabo, A.L. Mohamed, T.A. Khattab, Preparation of cellulose-based electrospun fluorescent nanofibres doped with perylene encapsulated in silica nanoparticles for potential flexible electronics, *Luminescence* 37(1) (2022) 21-27.
- [30]. M. Rehan, S. Zaghlool, F.A. Mahmoud, A.S. Montaser, A. Hebeish, Design of multi-functional cotton gauze with antimicrobial and drug delivery properties, *Materials Science and Engineering: C* 80 (2017) 29-37.
- [31]. M.M. Abd El-Hady, A. Farouk, S.E.-S. Saeed, S. Zaghlool, Antibacterial and UV protection properties of modified cotton fabric using a curcumin/TiO₂ nanocomposite for medical textile applications, *Polymers* 13(22) (2021) 4027.
- [32]. H.E. Emam, S. Zaghlool, H.B. Ahmed, Full ultraviolet shielding potency of highly durable cotton via self- implantation of palladium nanoclusters, *Cellulose* 29(8) (2022) 4787-4804.
- [33]. E.M. Reda, H.A. Othman, H. Ghazal, A.G. Hassabo, Kinetic and isothermal study of dye absorption using pre-treated natural fabrics using polyamine compounds, *Scientific Reports* 15(1) (2025) Article number: 3794.
- [34]. M. Er-Rafik, A.L. Mohamed, M. Möller, K. Spyropoulos, R. Wagner, Advanced textile enhancers- magnasoft silq[®]: Investigation of the deposition onto cotton fibers, *Melliand Inter.* 5(47-54) (2012) 3157.
- [35]. A.G. Hassabo, A. Mendrek, C. Popescu, H. Keul, M. Möller, Deposition of functionalized polyethylenimine-dye onto cotton and wool fibres, *RJTA* 18(1) (2014) 36-49.
- [36]. A.L. Mohamed, A.G. Hassabo, Engineered carbohydrate based material/silane as a thermo and pH-sensitive nanogel containing zinc oxide nanoparticles for antibacterial textile, *International Conference on Medical Textiles and Healthcare Products (MedTex 2015)*, Department of Material and Commodity Sciences and Textile Metrology, Faculty of Material Technologies and Textile Design, Lodz University of Technology, Lodz, Poland, 2015.
- [37]. H.E. Emam, A.L. Mohamed, Controllable release of povidone-iodine from networked pectin@carboxymethyl pullulan hydrogel, *Polymers* 13 (2021) 3118(1-21).
- [38]. N. Kannan, M.M. Sundaram, Kinetics and mechanism of removal of methylene blue by adsorption on various carbons--a comparative study, *Dyes Pigm.* 51(1) (2001) 25-40.
- [39]. Y.S. Ho, D.A.J. Wase, C.F. Forster, Kinetic studies of competitive heavy metal adsorption by sphagnum moss peat, *Environmental Technology* 17(1) (1996) 71-77.
- [40]. X. Xu, B.-Y. Gao, Q.-Y. Yue, Q.-Q. Zhong, Preparation and utilization of wheat straw bearing amine groups for the sorption of acid and reactive dyes from aqueous solutions, *Journal of Hazardous Materials* 182(1-3) (2010) 1-9.
- [41]. D. Caparkaya, L. Cavas, Biosorption of methylene blue by a brown alga *Cystoseira barbatula* kützing *Acta Chimica Slovenica* 55 (2008) 547-553.
- [42]. A.G. Hassabo, *Synthesis and deposition of functional nano-materials on natural fibres* RWTH Aachen University, Germany, 2011, p. 154.
- [43]. S. Wang, Y. Boyjoo, A. Choueib, Z.H. Zhu, Removal of dyes from aqueous solution using fly ash and red mud, *Water Res.* 39(1) (2005) 129-138.
- [44]. F. Doulati Ardejani, K. Badii, N. Yousefi Limaee, S.Z. Shafaei, A.R. Mirhabibi, Adsorption of direct red 80 dye from aqueous solution onto almond shells: Effect of pH, initial concentration and shell type, *Journal of Hazardous Materials* 151(2-3) (2008) 730 - 737.
- [45]. A.O. Dada, A.P. Olalekan, A.M. Olatunya, O. DADA, Langmuir, freundlich, temkin and dubinin-radushkevich isotherms studies of equilibrium sorption of zn²⁺ unto phosphoric acid modified rice husk, *Journal of Applied Chemistry* 3(1) (2012) 38-45.
- [46]. B.H. Hameed, D.K. Mahmoud, A.L. Ahmad, Equilibrium modeling and kinetic studies on the adsorption of basic dye by a low-cost adsorbent: Coconut (cocos nucifera) bunch waste, *Journal of Hazardous Materials* 158(1) (2008) 65-72.